ECCOMAS Congress 2016
VII European Congress on Computational Methods in Applied Sciences and Engineering
M. Papadrakakis, V. Papadopoulos, G. Stefanou, V. Plevris (eds.)
Crete Island, Greece, 5–10 June 2016

# EFFECT OF DISC GEOMETRY ON THE DYNAMIC STABILITY OF DIRECT SPRING OPERATED PRESSURE RELIEF VALVES (ECCOMAS CONGRESS 2016)

**István Erdődi**[1], **Csaba Hős**[1]

[1]Budapest University of Technology and Economics
Department of Hydrodynamic Systems
1111 Budapest, Műegyetem rkp. 7-9.
e-mail: ierdodi@hds.bme.hu, cshos@hds.bme.hu

**Keywords:** pressure relief valve, dynamic stability, computational fluid dynamics, reduced order modelling

**Abstract.** *The most important parameter of a direct spring operated pressure relief valve is its capacity, which is the rated flow through the valve under conditions given by the corresponding industrial standard. There are several phenomena due to which dynamic instabilities may arise in the system, leading to dangerous oscillations and reduced flow rate. One of the causes of these instabilities is the acoustic coupling of the valve with its upstream piping, the mathematical background of which has already been thoroughly investigated by the researchers at our department. As a continuation of that work, this paper focuses on the engineering applications by proposing various valve disc geometries based on preliminary measurement results, and evaluating their dynamic stability performance in a wide range of parameters. Steady-state CFD computations were performed to determine the mass flow rate and force characteristics of the various valve discs. Through these quantities, the behaviour of each geometry was implemented into our one-dimensional coupled gas dynamical solver, which resolves the pipe dynamics using the one-dimensional continuity-, momentum- and energy equations. The valve itself is modelled as a one degree-of-freedom oscillator. Finally, the stability maps of each geometries were calculated using the gas dynamical model and it was shown that the shape of the fluid force function does indeed have a significant effect on the stable operating range.*

## 1 INTRODUCTION

The main purpose of pressure relief valves is to guarantee that the pressure in the protected system does not exceed a prescribed level, which is the *set pressure* of the valve. The other important parameter is the so-called *capacity*, that is the rated flow through the valve under stated conditions prescribed by the corresponding standard [1]. As this determines how quick the relief process is, it is imperative from the point of safety that this mass flow rate is guaranteed. However, certain instabilities may arise, leading to harmful vibrations and a reduction in the flow rate.

The literature distinguishes between static and dynamic instabilities. The former involves the study of the governing equations of the valve — usually in a linearised form — around its equilibrium positions [2], while the latter deals with more complicated, generally system-level issues [3]. In this paper a dynamic instability caused by the acoustic coupling between the valve and the straight upstream piping is investigated. Previous measurements and simulation results have shown that the stability in this case depends on the driving mass flow rate and the length of the upstream piping for a given valve geometry [4, 5]. The goal of this paper is to provide a numerical method for stability analysis, and also to get an insight into the geometry-dependence of this instability by qualitatively comparing the stability maps in the mass flow rate and pipe length plane for three different valve disc geometries.

## 2 THEORETICAL BACKGROUND

The valve disc can be modelled as a one degree-of-freedom oscillator, for which the equation of motion is

$$m\ddot{x}_\mathrm{v} + k\dot{x}_\mathrm{v} + s(x_\mathrm{v} + x_\mathrm{p}) = F_\mathrm{total}, \tag{1}$$

where $m$ is the reduced mass of the moving parts, $x_\mathrm{v}$ is the valve lift, $k$ is the damping coefficient, $s$ is the spring stiffness, $x_\mathrm{p}$ is the pre-compression of the spring and $F_\mathrm{total}$ is the total force acting on the valve disc. The latter is the sum of the pressure, momentum and viscous forces — its modelling poses a significant challenge, as the momentum and viscous components cannot be accurately approximated by analytical means without a detailed knowledge of the flow-field. To circumvent this, the so-called effective area was employed during our calculations [6, 7, 8], that is

$$F_\mathrm{total} = A_\mathrm{eff}(x_\mathrm{v})(p_\mathrm{v} - p_\mathrm{b}), \tag{2}$$

where $A_\mathrm{eff}(x_\mathrm{v})$ is the effective area function, $p_\mathrm{v}$ is the pressure upstream of the valve and $p_\mathrm{b}$ is the back pressure. This assumes that the total force can be expressed by multiplying the pressure drop on the valve by an equivalent area, which depends only on the valve lift. Note that this approach neglects any unsteady effects, such as those from a non-zero valve velocity. The effective area functions differ for all valve geometries, and as such these are unknown as of now. However, since both the momentum and viscous forces equal zero if the valve is in a closed position, the effective area at that point equals the cross-sectional area of the seat.

During dynamically unstable cases, it is possible that the valve hits the seat. The resultant impact is treated as a mapping in the model with

$$\dot{x}_\mathrm{v}{}^{+} = -r\dot{x}_\mathrm{v}{}^{-}, \tag{3}$$

where $\dot{x}_\mathrm{v}{}^{-}$ and $\dot{x}_\mathrm{v}{}^{+}$ are the valve velocities before and after the impact and $r$ is the coefficient of restitution. For convenience, let the seat be located at $x_\mathrm{v} = 0$. Bouncing occurs if the valve velocity is above a set threshold ($\dot{x}_\mathrm{v}^{-} \geq \dot{x}_\mathrm{th}$), or the velocity is lower than the threshold and the

sum of all forces pushes the valve away from the seat ($\dot{x}_\mathrm{v}^- < \dot{x}_\mathrm{th}$ and $\ddot{x}_\mathrm{v}^- > 0$). Otherwise, the valve sticks to the seat.

The one-dimensional continuity-, momentum-, and energy equations were written for the straight pipe section upstream of the valve, which are

$$\frac{\partial \mathbf{U}}{\partial t} + \frac{\partial \mathbf{F}}{\partial \xi} = \mathbf{Q}, \tag{4}$$

$$\mathbf{U} = \begin{pmatrix} \rho \\ \rho v \\ \rho e \end{pmatrix}, \quad \mathbf{F} = \begin{pmatrix} \rho v \\ \rho v^2 + p \\ \rho v e + p v \end{pmatrix}, \quad \mathbf{Q} = \begin{pmatrix} 0 \\ -\frac{f(v)\rho}{2D_\mathrm{pipe}} v|v| \\ 0 \end{pmatrix},$$

where $t$ is the time, $\xi$ is the spatial coordinate, $\rho$ is the density, $v$ is the velocity, $e$ is the specific energy, $f$ is the Darcy friction factor and $D_\mathrm{pipe}$ is the diameter of the pipe. Preliminary tests have shown that treating the friction factor as a constant led to the erroneous estimation of the pressure drop due to the wide Reynolds number range in the pipe, and as such Blasius' correlation for turbulent flows was implemented — this means that the friction factor is a function of the velocity.

At the $\xi = 0$ end an infinitely large reservoir boundary condition was set, which is realized by prescribing the total pressure in the case of inflow to the pipe, and the static pressure otherwise. The valve boundary condition is implemented at $\xi = L$. The basic principle is that the mass flow rate leaving the pipe must also satisfy the discharge equation for the valve. If the flow is chocked, the equation to be solved is

$$\rho(L,t) A_\mathrm{pipe} v(L,t) = C_\mathrm{D} A_\mathrm{ref}(x_\mathrm{v}) \sqrt{\gamma \rho(L,t) p(L,t) \left(\frac{2}{\gamma+1}\right)^{\frac{\gamma+1}{\gamma-1}}}, \tag{5}$$

where $C_\mathrm{D}$ is the discharge coefficient, $A_\mathrm{ref}$ is the reference flow-through area and $\gamma$ is the ratio of specific heats. Similarly, for the non-chocked case we have

$$\rho(L,t) A_\mathrm{pipe} v(L,t) = C_\mathrm{D} A_\mathrm{ref}(x_\mathrm{v}) \sqrt{2\rho(L,t) p(L,t) \frac{\gamma}{\gamma-1} \left( \left(\frac{p_\mathrm{b}}{p(L,t)}\right)^{\frac{2}{\gamma}} - \left(\frac{p_\mathrm{b}}{p(L,t)}\right)^{\frac{\gamma+1}{\gamma}} \right)}. \tag{6}$$

The discharge coefficient is unknown as of yet, while the cylindrical surface between the seat and the valve disc is taken as the reference area is, that is

$$A_\mathrm{ref}(x_\mathrm{v}) = D_\mathrm{seat} \pi x_\mathrm{v}, \tag{7}$$

where $D_\mathrm{seat}$ is the diameter at the seat. In our case the seat was the chamfered pipe end, therefore $D_\mathrm{seat} = D_\mathrm{pipe}$ (see Figure 1(a)).

Equation (1) is solved using standard Runge-Kutta, while the Lax-Wendroff method is used for the discretization of equation (4). The boundary conditions were implemented with the isentropic method of characteristics.

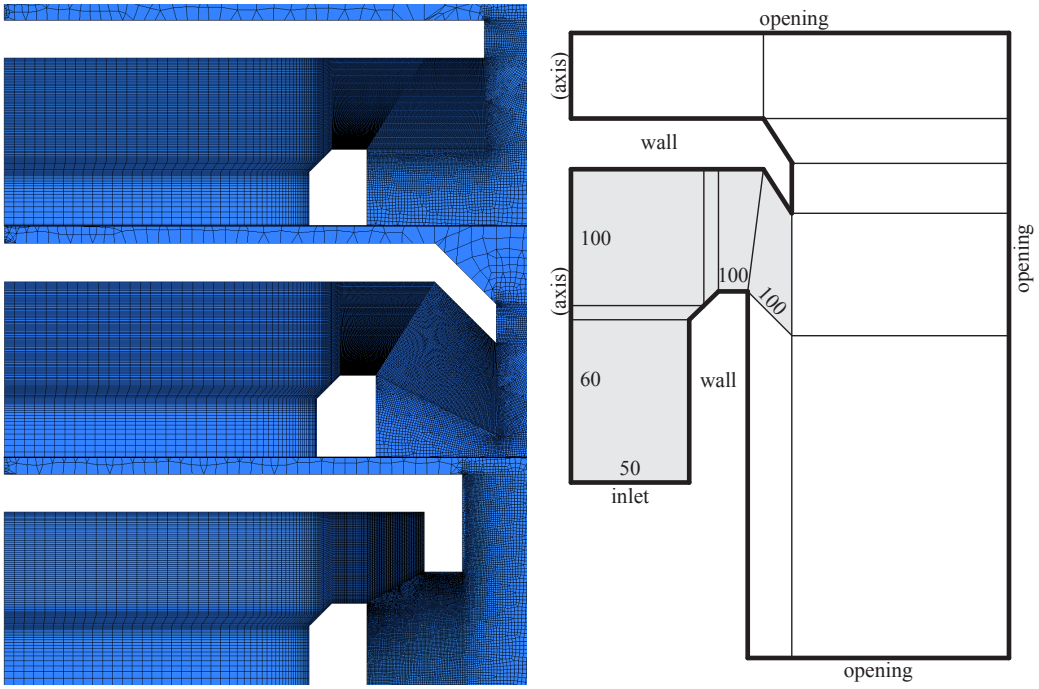


(a) (b)

Figure 1: (a) The three geometries ($0°$, $45°$ and $90°$ from top to bottom) with the mesh lines at a valve lift of $0.15D_{\text{pipe}}$. (b) The number of nodes and the boundary conditions. The filled parts indicate the structured part of the mesh. (The figure is not proportional for illustration purposes.)

## 3 CFD SETUP

As mentioned in the previous section, two necessary parameters are unknown due to the lack of accurate analytical methods: the effective area function and the discharge coefficient. Their values were determined by means of CFD.

Simulations were conducted for three different geometries, which were generated by varying the collar angle (Figure 1(a)). Axisymmetric treatment of the flow field was possible due to the simplicity of the geometry, effectively rendering the problem two-dimensional and as such significantly reducing the needed computational time. This resulted in a wedge-shaped domain with a central angle of $5°$, meaning that the extensive quantities — namely the mass flow rate and the total force acting on the valve — had to be rescaled for the full-sized valve.

The meshes were automatically generated for all geometries and lifts, with the number of nodes varying between $80\,000$ and $85\,000$. They consist of both structured and unstructured regions according to Figure 1(b) (the modelled domain is similar for the $0°$ and $90°$ cases). The meshes were created in ICEM. The inner diameter of the pipe was $40.2\,\text{mm}$, the upstream piping had a length of $10D_{\text{pipe}}$ and the valve lift was varied between $0.05D_{\text{pipe}}$ and $0.30D_{\text{pipe}}$.

Total pressures between $2$ and $6\,\text{bar}$ were prescribed at the inlet boundary condition with a static temperature of $293\,\text{K}$. The pressure was set to $1\,\text{bar}$ at the opening boundary condition, which corresponds to static or total pressure for outflow and inflow, respectively. The temperature was also $293\,\text{K}$. The medium was air with the ideal gas law and the k-$\epsilon$ turbulence model. The simulations were done in CFX environment. The High Resolution scheme was employed for the advection terms and the turbulence model, and the Second Order Backward Euler for

| | | |
|---|---|---|
| Pipe diameter | $D_{\text{pipe}}$ | 40.2 mm |
| Relative pipe length | $\frac{L}{D_{\text{pipe}}}$ | varied |
| Reduced mass | $m$ | 1 kg |
| Spring stiffness | $s$ | 21000 N/m |
| Discharge coefficient | $C_{\text{D}}$ | geometry-dependent |
| Gas constant | $R$ | 287 J/(kgK) |
| Ratio of specific heats | $\gamma$ | 1.4 |
| Kinematic viscosity | $\nu$ | $1.511 \times 10^{-5}\text{m}^2/\text{s}$ |
| Set pressure | $p_{\text{set}}$ | 3 bar |
| Inlet total pressure | $p_{\text{tot,r}}$ | varied |
| Inlet static temperature | $T_{\text{r}}$ | 293 K |
| Back pressure | $p_{\text{b}}$ | 1 bar |
| Environmental temperature | $T_0$ | 293 K |
| Initial relative valve lift | $\bar{x}(0)$ | 20 |
| Initial valve velocity | $\dot{x}(0)$ | 0 $\frac{\text{m}}{\text{s}}$ |
| Spatial resolution | $n_x$ | 10 |

Table 1: Parameter values

the time stepping. A mesh dependency study was concluded at the lowest and largest valve lifts with the highest inlet total pressure by doubling the mesh resolution on all edges, i.e. quadrupling the number of elements. The relative differences for both the fluid forces and the mass flow rates were below one percent, therefore the results on the original mesh can be deemed as numerically accurate.

The mass flow rates, the pressures at the seat and the total forces acting on the valve disc were extracted from the simulation results. With them, both the discharge coefficients and the effective area functions were determined for all three geometries using Equations (2) and (5).

## 4 RESULTS

The gas dynamical model consisting of Equations (1) and (4) was solved with the parameters listed in Table 1. To create the stability maps, the inlet total pressure was varied between $3.1$ and $3.4$ bar with increments of $1250\,\text{Pa}$, and the upstream pipe length was varied between $20D_{\text{pipe}}$ and $40D_{\text{pipe}}$ with increments of $0.5D_{\text{pipe}}$. The effective area functions and the discharge coefficients were set based on the fixed-lift CFD simulation results. The former are illustrated in Figure 2, which also shows the functions for incompressible simulations on the same geometries. The error bars represent the dependence on the pressure at the pipe end. The effective area values are the lowest for the $0^\circ$ geometry, which is expected since it has the lowest jet deflection angle — however, the $90^\circ$ results are only higher than the $45^\circ$ ones for lower lifts. It can also be seen that the pressure-dependence is much lower in the incompressible and that compressibility has a strong effect both qualitatively and quantitatively. Note that the incompressible effective areas served only illustrational purposes, all calculations were made with the compressible results. The discharge coefficients were

$$C_{\text{D},0^\circ} = 0.8545, \quad C_{\text{D},45^\circ} = 0.8515, \quad C_{\text{D},90^\circ} = 0.7787. \tag{8}$$

These values indicate that the $90^\circ$ geometry had a significant choking effect, reducing the mass flow rate under similar conditions by around $10\%$.

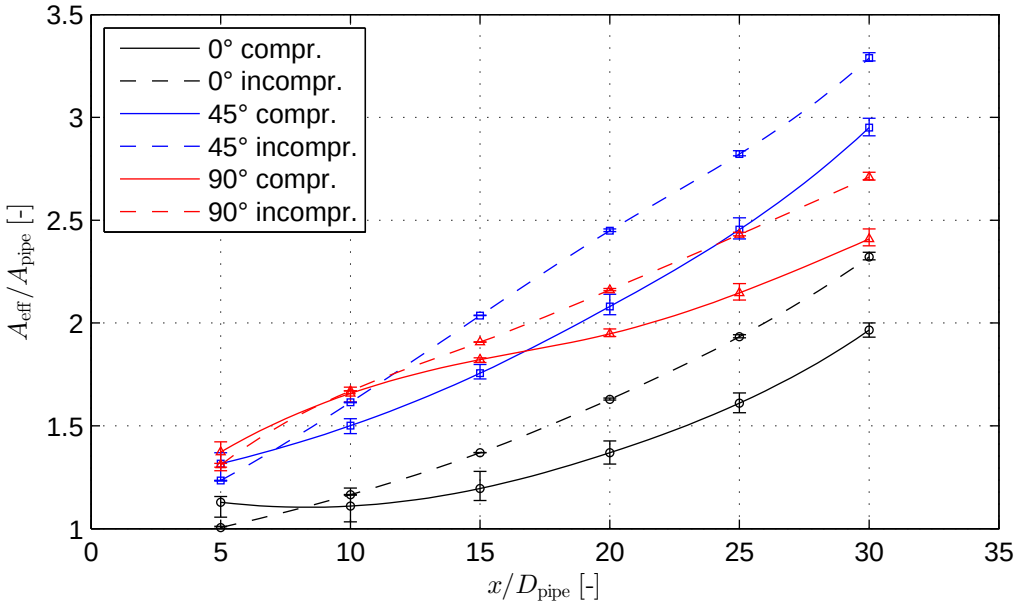


Figure 2: The effective area results for both the compressible (continuous lines) and incompressible (dashed lines) cases.

The results were said to be stable if the valve lift reached the equilibrium position in a decaying manner, and unstable otherwise, i.e. when periodic non-decaying oscillations were produced. First, the stability map was created in the inlet total pressure and upstream pipe length plane, as these were the two varied parameters (Figure 3(a)). The boundary curves differ in the three cases: for the $0°$ geometry, increasing the inlet total pressure extends the stable operating range, while the system behaves the opposite way for the $45°$ disc. In the case of the $90\,\text{deg}$ geometry, the boundary of stability is seemingly independent of the inlet total pressure. This shows that the accurate calculation of the fluid forces introduces not just qualitative, but also quantitative differences in regarding the boundary of stability.

The corresponding industrial standard [1] and the literature [9] usually discusses stability as a function the driving mass flow rate and pipe length. This map can be seen in Figure 3(b). Similar tendencies can be observed to those mentioned above regarding the shape of the curves, however, the difference in the mass flow rates makes the comparison ambiguous — it is possible that at higher flow rates the $0°$ curve becomes flatter (or even decreasing). The lower flow rates can be traced back to the lower effective area values (see Figure 2) as lower fluid forces do not produce as much valve lift.

## 5 CONCLUSIONS

This study employed a relatively simple, one-dimensional model for computing the valve response for a given inlet total pressure. Steady-state CFD simulations were conducted for three different valve disc geometries in order to obtain their force characteristics and discharge coefficients. With these, their specifics were implemented into the reduced model and a parameter study was conducted in the mass flow rate and the inlet total pressure plane. It was shown that even slight changes in the disc geometry can have a significant effect on both the stable operating range and the resulting mass flow rate.

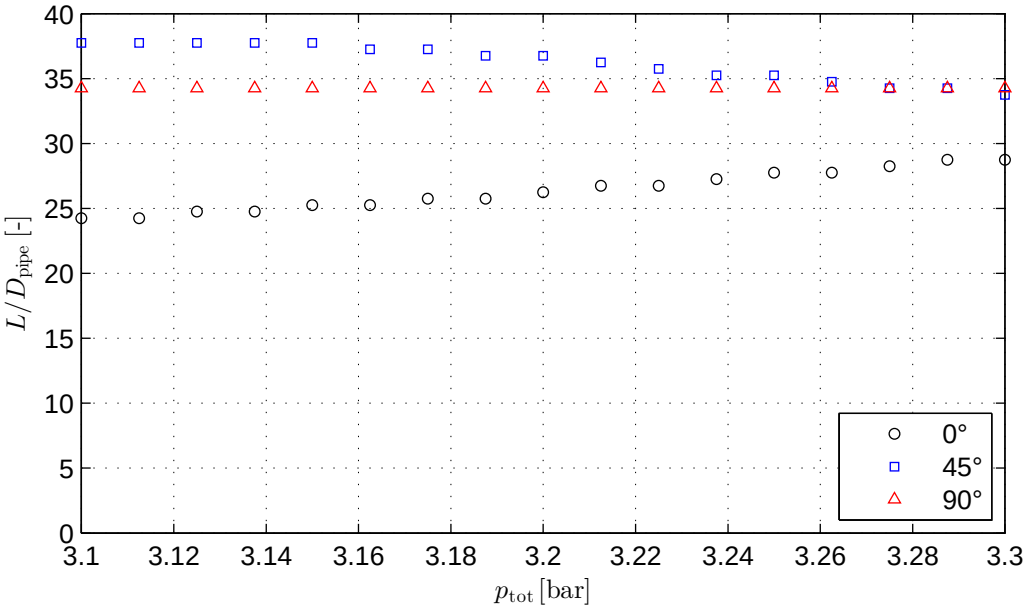


(a)

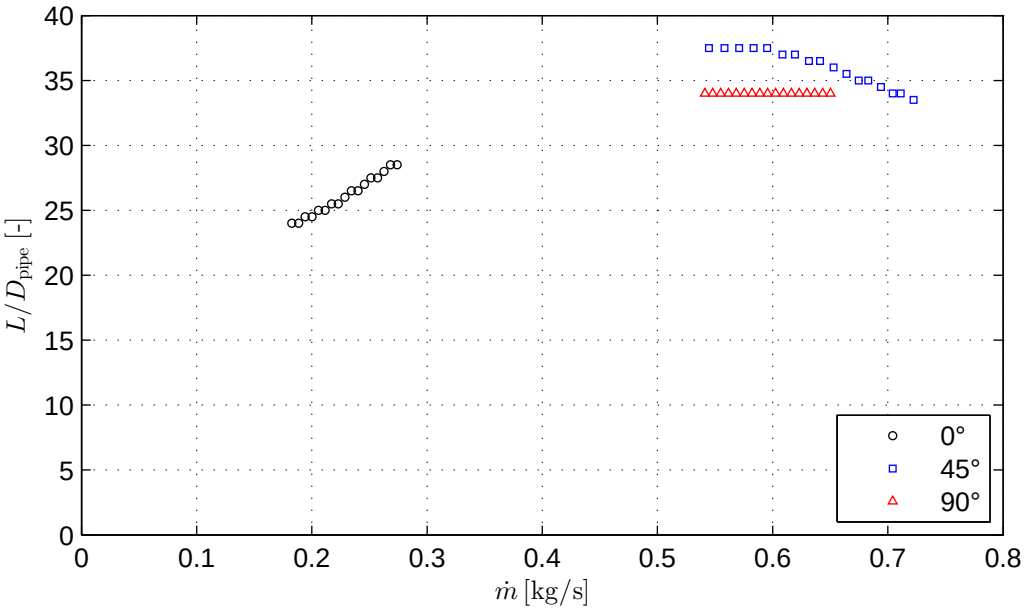


(b)

Figure 3: Boundaries of stability in the total pressure and pipe length (a) and mass flow rate and pipe length (b) planes. In both cases instability was observed above the boundaries.

## 6 ACKNOWLEDGEMENTS

This project was supported by the OTKA Grant K116549 of Csaba Hős. The authors would also like to express their thanks to Zalán Búcsú and Szabolcs Sánta for providing their incompressible simulation results and numerical meshes.

## REFERENCES

[1] American Petroleum Institute, "API Standard 520: Sizing, Selection, and Installation of Pressure-relieving Devices, Part II—Installation," 2015.

[2] C. Bazsó and C. Hős, "On the static instability of liquid poppet valves," *Periodica Polytechnica Mechanical Engineering*, vol. 59, no. 1, pp. 1–7, 2015.

[3] C. B. Domnick, F.-K. Benra, D. Brillert, and C. Musch, "Modification of a steam valve diffuser for enhanced full load and part load operation using numerical methods," in *Proceedings of CMFF'15*, (Budapest), 2015.

[4] A. Beune, J. Kuerten, and M. van Heumen, "CFD analysis with fluid-structure interaction of opening high-pressure safety valves," *Computers and Fluids*, vol. 64, pp. 108–116, 2012.

[5] O. Frommann and L. Friedel, "Analysis of safety relief valve chatter induced by pressure waves in gas flow," *Journal of Loss Prevention in the Process Industries*, vol. 11, no. 4, pp. 279–290, 1998.

[6] V. Dossena, F. Marinoni, F. Bassi, N. Franchina, and M. Savini, "Numerical and experimental investigation on the performance of safety valves operating with different gases," *International Journal of Pressure Vessels and Piping*, vol. 104, pp. 21–29, 2013.

[7] C. J. Hős, A. R. Champneys, K. Paul, and M. McNeely, "Dynamic behavior of direct spring loaded pressure relief valves in gas service: Model development, measurements and instability mechanisms," *Journal of Loss Prevention in the Process Industries*, vol. 31, no. 1, pp. 70–81, 2014.

[8] P. Moussou, R. J. Gibert, G. Brasseur, C. Teygeman, J. Ferrari, and J. F. Rit, "Instability of pressure relief valves in water pipes," *Journal of Pressure Vessel Technology*, vol. 132, no. 4, p. 041308, 2010.

[9] C. Hős, A. Champneys, K. Paul, and M. McNeely, "Dynamic behaviour of direct spring loaded pressure relief valves in gas service: II reduced order modelling," *Journal of Loss Prevention in the Process Industries*, vol. 36, pp. 1–12, 2015.